Single-cell Growth Rate Variability in Balanced Exponential Growth

Kuheli Biswas,[1,2] Amy E. Sanderson,[3] Hanna Salman,[3,4] and Naama Brenner[1,2]

[1] *Department of Chemical Engineering, Technion, Israel Institute of Technology, 32000 Haifa, Israel*

[2] *Network Biology Research Lab, Technion, Israel Institute of Technology, 32000 Haifa, Israel*

[3] *Department of Physics and Astronomy, University of Pittsburgh, Pittsburgh, PA 15260*

[4] *Department of Computational and Systems Biology, University of Pittsburgh, Pittsburgh, PA 15260*

Exponential accumulation of cell size and highly expressed proteins is observed in many bacterial species at the single cell level. Exponential rates exhibit cycle-by-cycle fluctuations and correlation across components - different proteins and cell size. In such balanced growth, homeostasis of all variables is maintained simultaneously. In this study, we examine the phenomenological features of growth-rate variability and present a theoretical framework to explain them and the emergence of multi-variable homeostasis. Our findings suggest that homeostasis results from the emergence of a high-dimensional dynamic attractor supporting balanced exponential growth. The stability of this attractor leads to a decay in instantaneous growth rate noise throughout the cell cycle, aligning with empirical findings. We also correctly predict that cells with higher growth rates experience a faster decay in growth rate noise. Surprisingly, our analysis identifies noise generated by uneven cell division as the primary source of variability in growth rates. The theory offers a clear explanation for many observations, validated against extensive single-cell data. The emergence of homeostasis spontaneously from dynamic interactions suggests that specific control mechanisms correcting deviations from a target may be unnecessary.

Introduction

Biological cells are variable in practically every property measured, including size, shape, protein content, metabolic activity, and more. Such phenotypic variability is seen even for simple isogenic cells such as bacteria living in a well-controlled homogeneous environment. Early studies, viewing these cells under a microscope, already revealed that their size and division times span a distribution, and their statistical nature was measured and modeled (1, 2). In recent decades, such studies have advanced tremendously with the development of single-cell experimental techniques and accompanying statistical theory.

The fluorescent marking of proteins enabled the direct study of specific gene expression levels. These studies showed that even functionally essential genes, thought to be under tight regulation, are expressed with broad variability across a population. While number fluctuations could explain variability in low-copy-number cellular constituents, highly expressed genes and highly abundant components, as well as cell size itself, are holistic integrated properties whose variability is more difficult to account for by a single source (3, 4). Nevertheless, a coherent phenomenology of their statistical properties in microbial populations has emerged recently through multiple studies. Highly expressed proteins generally exhibit a broad and skewed distribution, with a universal shape

found in many microorganisms (5). These distributions are log-normal-like (6–8), and characterized by a quadratic scaling between mean and variance (5, 9). Cell size exhibits universal statistical properties similar to those of proteins, with the same log-normal-like universal distribution shape (7, 8, 10).

Dynamic measurements of single-cell growth and division data enabled the comparison between population and temporal statistics. Both were found to exhibit the same universal distribution shape and moment scaling (8). These data also revealed that approximately exponential accumulation of highly abundant proteins and cell size is common among several types of bacteria (8, 9, 11–19). The dynamic variables - exponential accumulation rates, times between consecutive divisions, and even division fractions - fluctuate considerably across cycles, and their distributions and correlations were measured (20). Such quantitative data opened the door to the development of coarse-grained stochastic models which account for the essential features of growth and division. These models were applied (separately) to cell size and abundant proteins and successfully predicted their statistical properties (7, 21, 22). Interestingly, the same model applies equally well to different components and cell size (10).

In the current work, we focus on the single-cell growth rate phenotype and its statistical and dynamic properties. While cell size and cycle times have been analyzed statistically for many decades and more extensively in recent years, the properties of single-cell growth rates have received less attention. These rates can be extracted from the multiple available experimental data sets where bacteria are grown in microfluidic devices for an extended time. A prominent feature of these rates is that despite fluctuations across consecutive cell cycles, in balanced exponential growth different accumulating components (such as distinct highly expressed proteins and cell size) exhibit strong correlations among their growth rates at the same cycle. Thus, understanding the statistical properties of growth rates leads us to adopt a multi-variable approach, which addresses the simultaneous homeostasis of different phenotypes in a holistic manner and their inter-correlations (8, 9, 16).

We first present the phenomenology of growth-rate fluctuations, both in terms of instantaneous and of cycle-averaged variables. Then, we combine multi-dimensional modeling and data analysis, to uncover the dominant underlying source of noise and the mechanism that controls and constrains it to ensure homeostasis. We find that homeostasis is induced by the emergence of a dynamic attractor of balanced exponential growth, a phenomenon that appears with little sensitivity to the exact interactions or number of components. The stability of such an attractor obviates the need for dedicated control mechanisms that compensate for deviations of specific variables from a target. Perhaps surprisingly, we identify noise in cell division - e.g. small deviations from symmetry in symmetrically dividing bacteria - as the dominant source of variability in growth rates. This picture explains a host of observations, tested on a collection of published single-cell data. We discuss the generality of our results and their implications, as well as future open questions.

Statistical and dynamical properties of growth rates

Single-cell experiments, which track growing and dividing cells for multiple generations, have revealed that biomass and highly expressed proteins accumulate approximately exponentially. An example is shown in Fig. 1a for one data set, depicting *E. coli*'s growth trajectories in a mother-machine microfluidic device. Exponential fits to both cell size and protein accumulation are in good agreement with the data, defining an effective growth rate (eGR) over the cell cycle. While deviations from exponential growth have been observed and studied (18, 23), the exponential approximation remains a compact and convenient description of single-cycle dynamics. The eGR varies from one cycle to the next for both of these properties, while their ratio - the protein concentration - fluctuates continuously over time over multiple cycles (lower panel in Fig. 1a). The balance between these different phenotypes across cycles of growth and division is manifested through the cycle-by-cycle correlation between the eGR of cell size and protein content (8, 9, 16, 18). An example of this correlation is displayed in Fig. 1b. This property is sometimes referred to as "balanced biosynthesis".

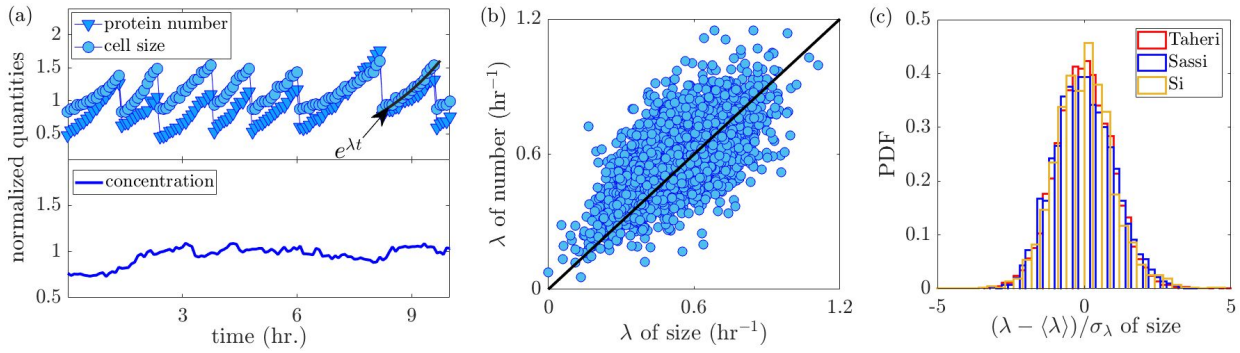

FIG. 1. ***E. coli* data : Exponential growth & balanced biosynthesis. (a)** Time traces of protein number (top, triangles), cell size (top, circles), and protein concentration (bottom, line), normalized by their respective means. The effective growth rates (eRG), λ, for cell size and protein number are estimated by fitting the dynamics during each cell cycle with exponential functions. An example of the fitting is shown for cell size (black curve in top panel), with $\lambda = 0.23$ hr^{-1} for cell size. **(b)** λs of cell size and of protein number show a strong correlation, with coefficient 0.64. **(c)** Probability Density Functions of cell size λ, normalized by their mean and standard deviation, for three different experiments on *E. coli*, showing a universal Gaussian-like shape. The Coefficients of Variation, (CV, standard deviation over mean) are different in each experiment: CV=0.05 (red;(13)), 0.18 (yellow; (17)), 0.3 (blue; (9)). Experimental details are in Table II.

The distribution of cell size eGR has consistently been reported Gaussian, as illustrated in Fig. 1c. However, the level of variability, quantified by the coefficient of variation (CV), changes significantly among published results, ranging from 5% to 40% across experiments (9, 12, 13, 16, 17, 19, 24). Our recent study has found that this level of eGR variability markedly affects the shape of division time distributions, accounting for its non-universal shape across experiments (10). However, the primary factors underlying eGR variability itself still remain unclear. Modeling work

has suggested several possible origins of these fluctuations, including the synthesis and degradation of cellular components, random distribution of mRNAs, and random deviations from symmetric division (25, 26). Identifying the dominant source of eGR variability has proven challenging; in particular, the large range of CV seen in different experiments, some of which performed in similar conditions, remains puzzling.

A complementary way to characterize single-cell growth in cell size or protein is by an instantaneous value across time, iGR, defined as the specific derivative - or the local relative rate of change. For purely exponential and deterministic growth, the iGR is constant over time and equal to the eGR. In measured data, where both deviations from a perfect exponential and noise exist, iGR fluctuates in time as seen in Fig. 2a. One may define the time-averaged iGR over a cycle duration, and this quantity is tightly correlated with the eGR. Fig. 2b shows that across cycles their distribution is very similar, and their cycle-by-cycle correlation is very high (0.87; inset).

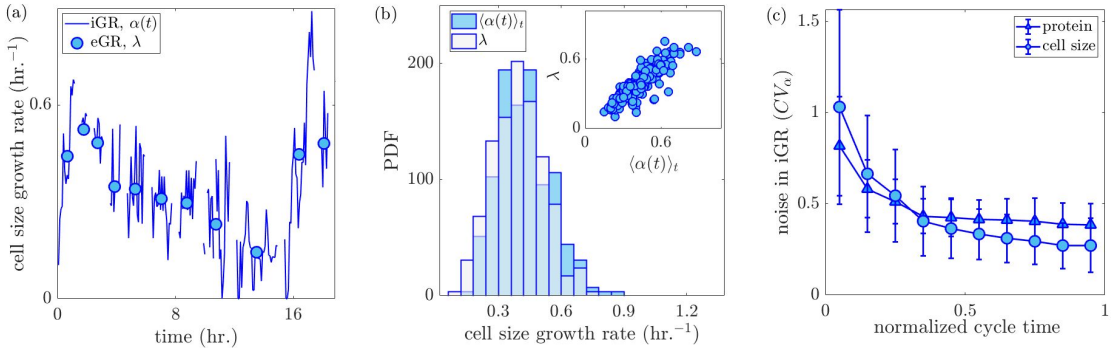

FIG. 2. ***E. coli* data (9): effective and instantaneous growth rates.** **(a)** iGR ($\alpha(t)$, blue line) and eGR (λ, blue circles) of cell size for several cycles. **(b)** Estimated probability density functions (PDFs) of λ and the time average of iGR over a cycle, $\langle\alpha(t)\rangle_t$ exhibit significant overlap. Mean of $\lambda = 0.47$ hr.$^{-1}$, standard deviation $= 0.12$ hr.$^{-1}$. Mean of $\langle\alpha(t)\rangle_t = 0.49$ hr.$^{-1}$, standard deviation $= 0.15$ hr.$^{-1}$. **Inset:** Scatterplot of λ vs. $\langle\alpha(t)\rangle_t$ collected from cell cycles of 10 lineages. Correlation coefficient ≈ 0.87. **(c)** CV across lineages at specific time points in the normalized cell cycle, for iGR of both cell size and protein number. For each cycle, normalized time was obtained by dividing absolute time by time at division, resulting in the scaling of normalized age from 0 to 1. The iGR conditioned on normalized cell cycle time was divided into 10 equal bins with bin width 0.1, and each bin's mean and standard deviation were estimated. CV = standard deviation divided by mean. This analysis was performed across 50 cell lineages, and the final plot represents the average CV with error bars indicating the standard deviation among the lineages. Experimental details are in Table II.

Although cells exhibit significant variability across growth and division cycles in all phenotypic quantities, they still maintain stability over multiple generations. This homeostasis is of much interest, and often considered related to control or regulation mechanisms that compensate for deviations from a set point over time. Modeling approaches that rely on eGR and describe the dynamics in discrete cell cycles, have considered control mechanisms that can compensate for fluctuations over a cycle, for example, adder or sizer mechanisms (7, 13, 27). The instantaneous

growth rate (iGR) allows observing variability across time at a finer resolution, within a single cycle. Recent work on *B. subtilis* has shown that variability in iGR among individual cycles decreases as the cell cycle progresses, interpreted as evidence for continuous regulation (18). We show in Fig. 2c that such a decrease appears for the iGR of both cell size and highly expressed protein in *E. coli*. These results suggest that some forces are continuously at work, not only at the end of the discrete cycle, to constrain variability in growth rate. In the subsequent discussion, we will demonstrate that these forces can emerge spontaneously in the presence of a dynamic attractor within the multi-component system. Therefore, it is not necessary to assume active control mechanisms that maintain specific variables around predetermined set points. This will emerge as part of a holistic dynamic picture that explains all aspects of the phenomenology described here. A general theoretic framework of balanced exponential growth, described next, will provide the context for this picture.

Models of balanced exponential growth

The emergence of balanced exponential growth, where many different components accumulate at the same exponential rate, was highlighted in a mathematical model already many years ago (28). This model describes a cyclic chain of linear kinetic reactions and is exactly solvable :at long times, one dominant positive eigenvalue determined the exponential increase of all components at the same rate. Although one specific model configuration was analyzed in detail, Hinshelwood noted that the main result was robust to details of the interaction topology and parameters. Later work studied arbitrary linear interaction networks, showing the same effect as long as the interaction matrix has at least one positive eigenvalue (16, 29).

Recent theoretic research significantly extended these results: it was shown that exponential growth with a single rate emerges in a broad class of models describing systems of non-linearly interacting components, such as chemical reaction networks (25, 30). For a general formulation, we imagine the cell as a container of volume $V(t)$ containing n components, with copy numbers $X_i,\ i = 1, 2...n$. Dynamics of the ith component is given by

$$\dot{X}_i = F_i(\mathbf{X}), \tag{1}$$

where F_i are nonlinear functions, representing the system's chemical reactions. The cell size is a linear combination of its components, $V(\mathbf{X}) = \sum_{i=1}^{n} \rho_i X_i$. In such a system, one finds the emergence of an asymptotic *exponential attractor* under the following condition on the functions $F_i(\mathbf{X})$:

$$F_i(\beta\mathbf{X}) = \beta F_i(\mathbf{X}) \quad \text{for any } \beta > 0. \tag{2}$$

The condition is obeyed by functions that describe mass-action kinetics and thus is very relevant to models of cellular interactions. An exponential attractor implies that all components and cell size grow exponentially at the same rate after a very long time (asymptotically). This exponential growth trajectory, although diverging to infinity, acts as a dynamic attractor to all initial

conditions in the following sense: starting from a nearby state, trajectories are attracted to the single-exponential growth manifold. While the appearance of an exponential attractor is universal in this class of models, the value of the asymptotic growth rate itself depends on the reactions and the parameters of the system.

On the attractor, when all system variables grow exponentially at the same rate, the ratios X_i/X_j, as well as the concentrations of all components, $Y_i = X_i/V$, remain fixed. Thus when considering this dynamical system in the space of concentrations instead of copy numbers, the exponential attractor becomes a fixed point with fixed concentrations. Writing Eq. (1) in terms of concentrations, $Y_i = X_i/V$, it contains the kinetic reactions and the effect of dilution by expanding volume:

$$\dot{Y}_i = \frac{1}{V} F_i(V\mathbf{Y}) - \alpha(t)\, Y_i, \tag{3}$$

where the volume growth rate, defined as

$$\alpha(t) = \frac{\dot{V}}{V} = \sum_{i=1}^{n} \rho_i F_i(\mathbf{Y(t)}), \tag{4}$$

is a function of all concentrations and is constant at the fixed point.

Several special case models in this class were studied previously (9, 25, 26, 31–33). Here, for a detailed analysis, we consider a concrete example involving a non-linear interaction network of three components: amino acids, metabolic enzymes, and ribosomes with respective population size X_{aa}, X_e, and X_r, as depicted in Fig. 3(a). The equations governing the system are

$$\dot{X}_{aa} = k_1 X_e - (k_2 + k_3)\frac{X_{aa}X_r}{V}, \tag{5a}$$

$$\dot{X}_e = k_2 \frac{X_{aa}X_r}{V}, \tag{5b}$$

$$\dot{X}_r = k_3 \frac{X_{aa}X_r}{V}, \tag{5c}$$

$$V(t) = \rho_{aa}X_{aa} + \rho_e X_e + \rho_r X_r. \tag{5d}$$

In this reaction network, amino acids are produced by the catalytic action of the metabolic enzyme from external food molecules with rate k_1. Metabolic and ribosomal proteins are synthesized from the amino acids in reactions catalyzed by ribosomes with rate k_2 and k_3, respectively. It is easily verified that the model obeys the scalability condition, and therefore exhibits an exponential attractor. The volume instantaneous growth rate, defined in Eq. 4, is computed for this system as

$$\alpha = \rho_{aa}(k_1 Y_e - (k_2 + k_3)Y_{aa}Y_r) + \rho_e k_2 Y_{aa}Y_r + \rho_r k_3 Y_{aa}Y_r. \tag{6}$$

On the exponential attractor, concentrations are fixed and we have an explicit expression for the growth rate common to all components (see Appendix B).

A remarkable property of the exponential attractor is that it is invariant to the division of all components by a constant fraction. Thus, precise division events where all components are multiplied by the same fraction f maintain concentrations and leave the trajectory on the exponential

attractor. The periodic occurrence of such division events can result in a finite stable attractor, composed of continuous growth and discrete divisions, such that a trajectory can be confined to the attractor for an infinite time. A crucial question from a realistic perspective is the attractor's stability to various noise sources, which we discuss next.

Stochastic sources of variability

Dynamics on the asymptotic exponential attractor is perturbed by non-ideal division events. To investigate this effect we implemented the deterministic growth model in simulation with cell divisions, where both the distribution of components among daughter cells and the condition for division are noisy. We assume that division fractions f for all components fluctuate around 1/2 (approximately symmetric division, independent among components), and that division occurs when cell size reaches a stochastic threshold C (other division mechanisms can be implemented with similar results, see Appendix D). Experimental histograms of threshold size and division fraction fit well with the Gaussian distributions, with typical coefficients of variation of $\mathrm{CV}_c \sim 5\% - 25\%$ for size threshold and $\mathrm{CV}_f \sim 5\% - 15\%$ for division fraction (9, 12, 13, 17–19, 24). These features are implemented in our model; we next explore how such fluctuations affect the dynamics, and specifically how they are regulated to ensure homeostasis in growth and division. Number fluctuations, that effectively turn the deterministic model itself into a set of discrete stochastic processes, will be discussed in a later section.

With the two noise sources described above, cell size and all cellular components still grow approximately exponentially during the cell cycle. Moreover, they maintain a form of balanced growth similar to that observed in experimental data (Fig. 3b): exponential rates fitted to the trajectories fluctuate across cycles and are correlated among different components - though not identical. The finite and relatively short time between consecutive divisions (where variables approximately double) has a major impact on the system's behavior. Noisy division constitutes a random perturbation that drives the trajectories away from the fixed point. During growth in the following cycle, it will be attracted back to the fixed point, but there may not be enough time before the next division to reach it. Examining the system in the space of concentrations, we find they fluctuate over time but remain around stable values (Fig. 3c). These fluctuations are composed of the discontinuous jumps of division, the "kicks" away from the fixed point, followed by continuous convergence back to it.

Fig. 3 d-f show these trajectories in three-dimensional concentration space. The stable attractor appears as a fixed point, and individual trajectories - shown with time coded by greyscale - start from random points away from the fixed point and are attracted to it during the cycle. As division noise increases, deviations are of larger magnitude, still followed by attraction to the fixed point, as evident in Fig. (3d-f). The stability of the fixed point can be analyzed from the eigenvalues of the Jacobian matrix at that point; we find that they are all real and negative (Appendix B), indicating global stability, as appears in the simulations. These results suggest that the system

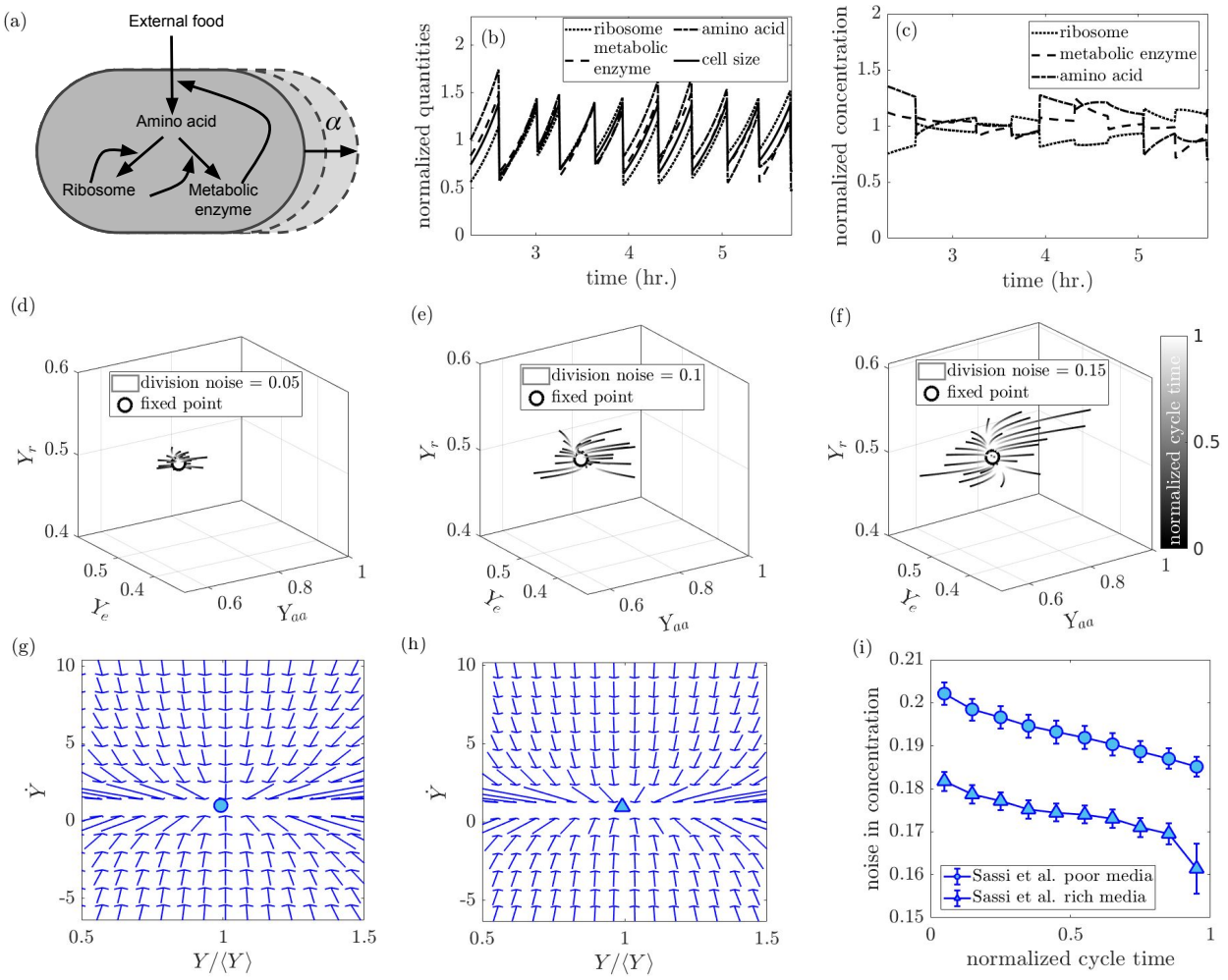

FIG. 3. **Dynamic attractor of growth and division in balanced exponential growth . (a)** Schematic of the model (Eqs. 5), describing the nonlinear reactions in a cell whose volume grows with rate α. The catalytic action of the metabolic enzyme on the external food source produces amino acids. Metabolic and ribosomal proteins are synthesized from amino acids in a reaction catalyzed by ribosomes. **(b)** Time traces of normalized cell size, component numbers, and **(c)** normalized concentrations with added noise in division fraction and division condition, respectively, $\mathrm{CV}_f = \mathrm{CV}_c = 0.15$. **(d-f)** Dynamics in concentration space of the three components, with division noise of $\mathrm{CV}_f = 0.05$, 0.1 and 0.15 while CV_c is fixed at 0.15. Trajectories are grayscale-coded by normalized cell cycle time from 0 (black, cycle start) to 1 (white, cycle end). The fixed point of the deterministic system is marked by a black circle. Initially, each trajectory deviates from the stable fixed point and converges towards it by the cycle's end. The extent of deviation increases with increasing CV_f (from d to f). Parameter values are in Table (I). Experimental data on *E. coli* (9) growing in nutrient **(g)** poor and **(h)** rich media: A flow map in concentration phase space, generated by discretizing Y and $\dot{Y}$ into 15 equally spaced bins. Arrows originate from the average values of Y and $\dot{Y}$ within each bin, with their directions and lengths determined by the differences between consecutive averages. Each vector is normalized to uniformly represent the directional field in the $Y - \dot{Y}$ phase plane, ensuring visual clarity without scaling distortions. The blue markers are the stable node attractors. **(i)** CV in concentration across normalized cell cycle time, for the same experiments as (g,h). Experimental details are provided in Appendix Table II.

as a whole obtains stability in the presence of noise from the underlying stable fixed point of the dynamics.

One may test this prediction by depicting the flow in phase-space directly from trajectory data (16). The fingerprints of the fixed point in 3-dimensional concentration space is manifested in the phase plane of one of the components, the $(Y, \dot{Y})$ plane, where Y is the concentration of a measured protein. Indeed, Fig. 3 g,h show two examples of such phase plane flow estimated from two experiments on E. coli (9).

The random deviation and relaxation back to the attractor will manifest itself as a decrease in variability between cycles in normalized time: each random division kicks the system in a different direction, but all converge to the same stable fixed point. This decay in concentration variability can be tested against experimental data, by normalizing the cycle time and estimating the variability across single cycles along this time. As shown in Fig. 3f, this variability indeed decreases along the normalized time.

Statistical properties of instantaneous growth rate (iGR)

In experimental measurements, access to multiple components' copy numbers and concentrations is typically limited to one or a few components. In the previous section we tested our predictions against a one-dimensional projection of one measured protein content. A different projection is obtained by considering growth rate: we recall that in the model, growth rate is a composite function of all concentrations (Eq. 4). Thus we can also test predictions of the high-dimensional model by using growth rate as a proxy and considering growth rate dynamics. Fig. 4a presents a sample trajectory of the one-dimensional cell size iGR dynamics in the model, with and without division noise. As expected, it is constant in the presence of deterministic symmetric divisions; with division noise, it deviates from its fixed-point value at the cycle starts and converges back during the cell cycle.

Figs. 4b, c depict the projected dynamics of iGR in the phase plane $(\alpha, \dot{\alpha})$, across varying division noise levels. Each division kicks the trajectory away from the fixed point in a random direction, inducing an initial deviation of iGR from the fixed point (black part of the trajectory), followed by continuous attraction back to the fixed point where $\dot{\alpha} = 0$ (open circles). The initial deviation increases with increasing division noise (panels b, c). The largest perturbation, Fig. 4c, reveals what appears to be a slow manifold with a shallow slope. This structure in the projected phase plane reflects the fixed point of the full system in higher dimensional concentration space, presented and analyzed in the previous section. Estimating the dynamic flow in the $(\alpha, \dot{\alpha})$ plane directly from experimental data, supports the picture of a fixed point also in this projection (Fig. 4e). Similar dynamics are also found in other experimental conditions, for example, a different nutrient composition or temperature (Appendix C Fig. S1).

The picture of attraction towards the fixed point suggests that iGR variability among individual cycles will be large immediately following division and will decrease during the continuous cycle,

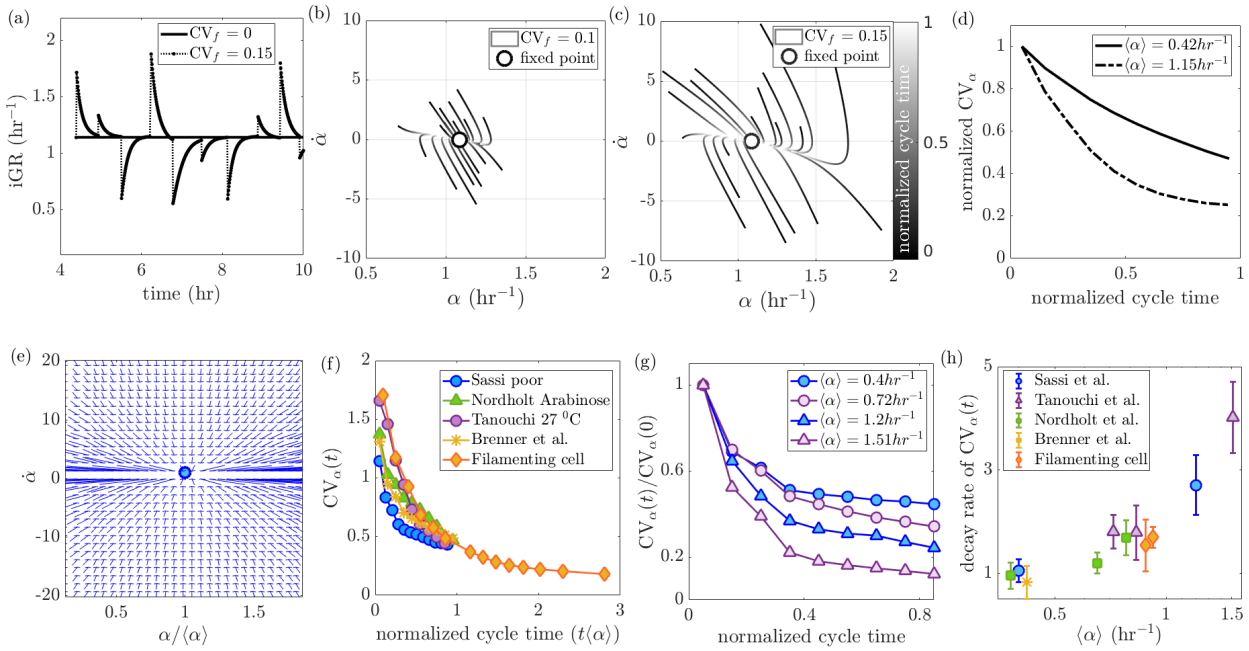

FIG. 4. **Model dynamics projected to iGR space (a-d) align with experimental data (e-h). (a)** iGR dynamics depicted without division noise ($\mathrm{CV}_f = 0$; solid line) and with noise (CV_f=0.15; dotted line), stabilizing at a fixed-point iGR value of $1.15hr^{-1}$. **(b), (c)** Trajectories in the $(\alpha, \dot{\alpha})$ phase space, with division noise $\mathrm{CV}_f = 0.1$ and 0.15, respectively. Greyscale code from cycle start (0, black) to cycle end (1, white), deviate from and return to the stable fixed point (black circle), with greater deviation at higher CV_f. Here $\mathrm{CV}c = 0$. **(d)** iGR noise, quantified by $\mathrm{CV}\alpha$, peaks at the cell cycle start and decays throughout, with faster decay in faster-growing cells ($\mathrm{CV}_c = 0$, $\mathrm{CV}_f = 0.15$). Model parameters are in Appendix Table I. **(e)** Estimated phase space flow from experimental data on *E. coli* (9) in iGR space. The map was created by discretizing α and $\dot{\alpha}$ into 30 bins, features arrows originating from the bin averages to show transitions between bins. Each vector is normalized to uniformly represent the directional field in the $(\alpha, \dot{\alpha})$ phase plane, ensuring no scaling distortion. The blue circle indicates a stable node attractor in this projection. **(f)** iGR noise ($\mathrm{CV}\alpha$) decreases along the cycle both for wild-type (blue (9), green (18), violet (12), yellow (8)) and filamenting cells (orange diamonds). To compare them, time was normalized by respective growth rate. Filamenting cells reach a lower iGR noise as they do not undergo division. Noise levels are quantified by segmenting the data into bins containing equal data points, calculating the standard deviation and mean of iGR within each bin, and computing their ratio. Experimental details on filamenting cells are given in Sec. F and wild-type dividing cells are provided in Table II. **(g)** Normalized iGR noise, adjusted by its initial value over a cycle, is analyzed using *E. coli* data across different nutrient conditions (poor: blue circles, rich: blue triangles) (9) and temperatures (27°C: violet circles, 37°C: violet triangles) (12). iGR noise decreases more rapidly in fast-growing cells. **(h)** The decay rate of iGR noise correlates positively with the mean iGR. This relationship is modeled by fitting an exponential curve to $CV_\alpha(t)$, and the resulting exponent quantifies the noise reduction rate, presented with confidence intervals (error bars).

reaching a minimum at its end. As in the case of the concentration above, we quantify iGR variability by the coefficient of variation across cycles in normalized time, $\mathrm{CV}_\alpha(t)$. In Fig. 4d,

we show that this quantity is maximal at the onset of the cell cycle and decreases monotonically towards its end.

Our model allows us to make also a more quantitative prediction on the rate of decrement of $\mathrm{CV}_\alpha(t)$. The speed of convergence back to the fixed point following a perturbation will be determined by the eigenvalues of the Jacobian matrix at this fixed point. Computing these eigenvalues as a function of model parameters shows that convergence is faster for growth conditions with higher α at the fixed point (see Appendix B). This in turn implies that $\mathrm{CV}_\alpha(t)$ will decrease more rapidly under conditions where the average growth rate is higher. Our model simulation demonstrates this effect, as shown in Fig. 4d.

We now have two qualitative predictions to compare to experimental data. The first, a decreasing variability of iGR across the normalized cell cycle, has already been observed in previous experimental work on *B. subtilis* (18). Similar behavior for *E. coli* across several different experimental conditions is also presented in Fig. 4f. The second prediction concerns the rate of decrease of $\mathrm{CV}_\alpha(t)$: from analysis of the model, Fig. 4d we expect a faster decrease in faster-growing cells compared to their slower-growing counterparts. This is also supported by *E. coli* data grown at different temperatures (12) and another in different nutrient conditions (9) (Fig. 4g). Quantifying the decay rate in iGR noise by fitting $CV_\alpha(t)$ to a decreasing exponential function, we analyzed a host of experimental data revealing that indeed this exponent increases with mean iGR, as shown in Fig. 4h.

Our analysis indicates that cell division is the primary disruption to the dynamic attractor. Consequently, another prediction is that halting cell division should extend the time of relaxation to the fixed point, thereby further reducing growth rate noise. We thus predict that filamenting cells that elongate without undergoing cytokinesis due to an inhibited division process will display reduced growth rate noise compared to normally dividing cells. This prediction is supported by recent findings published in (34), which corroborate our theory. Additionally, we provide new data on filamenting *E. coli* in Fig. 4f, further validating this prediction.

Statistical properties of effective growth rate (eGR):

The eGR, or effective growth rate λ, is empirically estimated by applying exponential fitting to cell size or protein content over the entire growth trajectory of the cell cycle. To a good approximation, it is the time average of the iGR over a cycle; see Appendix A. We have seen that empirically these two quantities have a very high correlation (inset Fig. 2b), and very similar distributions across cycles (Fig. 2b). We see this equivalence also in our model simulations (Fig. 5a). The model allows us to explore the dependence of eGR variability on different parameters; of particular interest are the division noise and the average growth rate.

Fig. 5b displays a greyscale map of CV_λ , the coefficient of variation of eGR, in the plane of division noise CV_f and average growth rate $\langle\lambda\rangle$. We find that CV_λ strongly varies with CV_f, but that the average growth rate has a much smaller effect. If relaxation rates were fixed, then

a higher average growth rate - associated with shorter cycle times - would result in less time to relax to the fixed point and thus higher variability among effective single-cycle rates. However, we have seen above that the relaxation rate actually scales with the mean growth rate, leaving a weak dependence of the variability CV_λ on $\langle\lambda\rangle$.

While it is clear that division noise affects eGR variability, there may be other noise sources contributing to it as well. The model simulations allow us to assess the relative importance of various noise sources on eGR variability: division noise, stochasticity in the threshold triggering division, and intrinsic number fluctuations in chemical reactions. Fig. 5c presents the outcomes for models with different noise sources: division noise only (solid line), a combination of division and threshold noise (dashed line), and with additional number fluctuations (dotted line). Notably, the impact of threshold noise on top of division noise is negligible. Consequently, the graphs representing only division noise and combined noise (solid and dashed lines, respectively) are visually indistinguishable. These findings align with those reported by (25). Number fluctuations

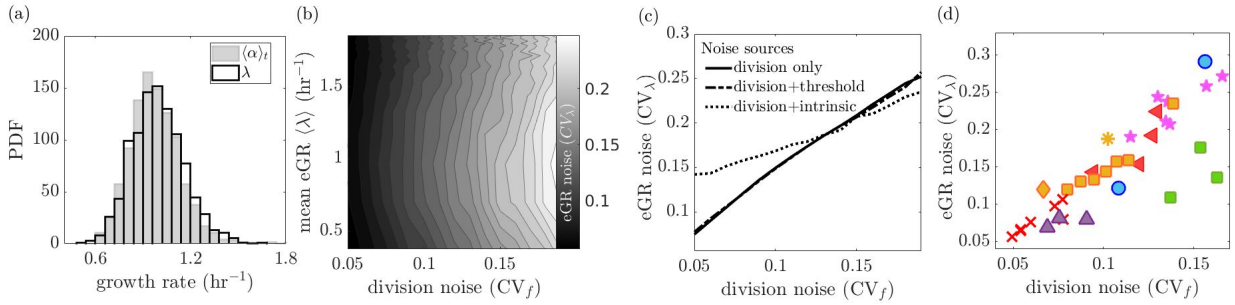

FIG. 5. **Uneven division is the major noise source in eGR: (a-c) Model simulation & (d) Data.** **(a)** PDFs $\langle\alpha(t)\rangle_t$ and λ show significant overlap with the same mean and variance while $\mathrm{CV}_f = 0.15$ and $\mathrm{CV}_c = 0$, i.e., deterministic threshold. **(b)** Variation of eGR noise (CV_λ) in the plane of average growth rate ($\langle\lambda\rangle$) and division noise (CV_f) for fixed threshold. **(c)** CV_λ increases monotonically with division noise CV_f for fixed $\langle\lambda\rangle = 1$, which exhibits no difference for $\mathrm{CV}_c = 0$ (solid line) and 0.15 (dashed line). This indicates that there is no effect of threshold noise on CV_λ. The effect of intrinsic noise, arising from number fluctuations, is represented by the dotted line. To incorporate this intrinsic noise we perform the Gillespie simulation (35) with exponentially distributed waiting times for each reaction in Eq. (5). **(d)** CV_λ from a range of different experimental data shows a tight positive correlation with the division noise, CV_f. The B. *subtilis* data are from (18) (green square). E. *coli* data are from (13) (red cross), (17) (red triangle), (12) (magenta triangle), (19) (magenta stars), (8) (yellow star), (24) (yellow square), filamenting cell data sec. F (yellow diamond). The model parameters and experimental details are presented in Tables I and II, respectively.

can also in principle contribute to noise in eGR. These fluctuations in the chemical dynamics result from the discreteness of molecular populations, taking values of non-negative integers instead of continuous variables, and each reaction has a probability of occurring instead of a rate. Eq. (5) is then replaced by its stochastic counterpart. A population variable that is a smooth exponential function of time in a deterministic simulation becomes a jagged function when intrinsic stochasticity

is switched on, and exponential fits give a different value of eGR in individual cycles. The results of this model, shown as a dotted line in Fig. 5c, show that number fluctuations become important for growth-rate variability in the region where division noise is very small. In the presence of significant division noise, number fluctuations add a small effect.

Taking a realistic value for division noise to be $\approx 10\%$ implies that division noise, arising from slight deviations from symmetric divisions, is the primary factor influencing fluctuations in growth rate. To test this prediction directly from data, we assembled a broad array of single-cell measurements and plotted the empirically estimated eGR noise - CV_λ - as a function of division noise, CV_f. Examining the dimensionless measure of noise allows us to incorporate a variety of experiments with different average growth rates into this figure. The result is displayed in Fig. 5d, revealing a striking correlation between these two measures, throughout a dynamic range where eGR noise changes by approximately a decade. The sharp decrease at very small division noise indicates that number fluctuations do not kick in this regime either, which is consistent with our focus on highly expressed proteins, where typically numbers are very large.

Discussion:

The mathematical foundation for understanding the sustained exponential growth observed in natural systems, such as cells with nonlinear reaction networks, has recently been elucidated (25, 30). A large class of models has been identified that exhibits asymptotic exponential growth of all components at the same rate; cell size is a weighted sum of these components, and grows at the same rate. These models are characterized by a crucial negative feedback loop between the accumulation of cell size and its constituents, thereby ensuring system stability and homeostasis. In this loop, the component serves as an activator that increases cell size, while their accumulation is in turn inhibited by dilution as cell size increases.

In the current work, we relied on the dynamic properties of the emerging collective attractor in such a system, to investigate the statistical properties of single-cell growth rate. This phenotype can be measured from growth trajectories either as a continuous logarithmic derivative of protein or cell size or as an effective coarse-grained fit over entire cell cycles. The two quantities are strongly related to each other - one is the average of the other - but because of their different nature, each sheds light on the underlying dynamical system from a different point of view.

From the mathematical framework of models supporting balanced exponential growth, we have learned that single-cell biomass growth rate is a compound phenotype that depends on the collective dynamics of many components. The instantaneous growth rate - iGR - of cell size depends on instantaneous changes in component concentrations. Therefore on the asymptotic attractor, where concentrations are fixed, the growth rate is common to all components and depends on system parameters. In the presence of noise, these growth rates are not identical but remain correlated.

Using a specific set of equations as our theoretical test case allowed us to explicitly calculate the attractor's properties: the unique growth rate associated with it and the linear-stability eigen-

values. This served as a basis to study the effect of various noise sources on the full system, in this case three-dimensional. The existence of a globally stable exponential attractor in the deterministic system has a major impact on the stochastic system; division noise constitutes discrete perturbations kicking the trajectories out of the attractor, while continuous growth during the cell cycle reflects their relaxation back to the attractor. The eigenvalues at the fixed point determine the timescales of relaxation.

Projecting the high-dimensional dynamical system onto the growth rate phase plane, provided three testable predictions on growth rate fluctuations. First, iGR fluctuations across cycles decrease over the cycle time. This is a fingerprint of the relaxation back to the constant-rate attractor following stochastic cell division. This phenomenon had already been reported in previous work on *B. subtilis*, but lacked an explanatory framework. Our picture of an underlying attractor, where division events kick the trajectory away and the continuous part of the cycle reflects relaxation back to the attractor, gives such a framework. We demonstrate the same behavior in several different experiments on *E. coli*, extending and generalizing the previous result.

Our analysis further makes the second prediction that iGR noise decreases faster in faster-growing cells. This follows from the theoretical result that the time scale of relaxation to the attractor increases with the attractor's mean growth rate (Fig. 4d). This finding is corroborated by empirical evidence in Fig. 4g. Additional data is presented in Fig. 4h.

Relaxation back to the stable fixed point following noisy division is manifested also in the behavior of two identified sister cells. While DNA is distributed evenly between the two sisters, other components are divided with approximately the same concentration, which leads to slightly higher reaction rates in the smaller cell. The two sisters will suffer opposing perturbations in growth rate, and after division will be attracted back to their common growth rate value. Thus the smaller sister's growth rate will increase following division and the larger one will decrease, as shown experimentally (36). This initial difference in iGR between sisters at the start of the cell cycle is diminished along the continuous part of their trajectories as both relax back to the common attractor.

It is natural to ask whether cell size, similar to growth rate, exhibits a parallel decrease in variability across normalized cell cycle time. Analysis of bacterial data reveals this is not the case; cell size mean and standard deviation increase along the cycle, and their ratio is mildly non-monotonic with similar features for all data sets tested (Appendix G, Fig. S4). In contrast, recent experiments on mammalian cells revealed a continuous decay in cell mass noise (37). The underlying cause of this essential difference between bacterial and mammalian cells is yet to be understood; it may be speculated that within a multi-cellular organism, control of cell size is of higher functional importance than in bacterial cells. The non-monotonic variability in bacterial cell size throughout the cell cycle also remains a topic for future investigation.

Using our model we examined the role of different noise sources - division noise, threshold noise, and number fluctuation - on eGR variability. The third prediction from our analysis is that of these

sources, division noise is the primary determinant of the growth rate noise. This prediction may initially seem surprising since division is considered quite symmetric in *E. coli* bacteria and the impact of division noise is often considered negligible. Indeed, in the presence of significant number fluctuations - which are relevant to cell components at very low copy numbers - this source of noise may be neglected. However, focusing on the highly expressed components that primarily make up the cell biomass, this turns out to be the dominant noise source affecting eGR. The reason is that noisy division kicks the dynamic trajectory off the exponential attractor, and fitting an exponential function to the cycle that relaxes back introduces a noisy effective growth rate (see also (16)). Remarkably, this prediction is borne out by the entire collection of data we analyzed, as presented in Fig. (5)d. Additional support is provided by the observation that filamenting cells exhibit a further decrease in growth rate noise as the growth cycle extends past the wild-type cells growth cycle (34) (Fig. 4f). Previous work has also reported that adding division noise to the model is essential for reproducing experimental growth rate variability (25).

Previous work on stochastic effects in cellular dynamics has tended to focus on number fluctuations. To connect with this line of research, we have simulated a previously studied linear model of balanced exponential growth: the Deterministic Hinshelwood Cycle (DHC) (28) and the Stochastic Hinshelwood Cycle (SHC) (21) (see Appendix E). The SHC model explicitly incorporates number fluctuations, also known as intrinsic noise or stochastic gene expression. A comparison reveals that both models exhibit the effect of the dynamic attractor with division perturbing the trajectories away, as shown in Appendix E, Fig. S3 (b), and (d). In the regime of division noise within the experimentally relevant range, the iGR noise in both SHC and DHC models are similar (see Fig. S3c), and so the PDF of the effective growth rates (Fig. S3e). This analysis of a different model is consistent with our conclusion that the primary contributor to growth rate variability is division noise.

The picture of a stable attractor underlying the dynamics of the many interacting cellular components sheds a different light on the question of noise, homeostasis, and control. Rather than dedicated active mechanisms to compensate for the accumulation of noise, it suggests that high-dimensional dynamics itself can induce stability across multiple division cycles. The interactions between components, and the negative multi-level feedback between cells and their components, ensure this homeostasis. This notion can potentially be very general and provide an alternative perspective to that of control theory, which is based on the direct estimation of cellular quantities, their comparison to setpoints, and their compensation against fluctuations. Further research is required to test the validity of this description of different cell types and conditions.

Acknowledgements: K.B. is supported by a fellowship from the Lady Davis Foundation at the Technion. The research is supported in part by the Israeli Science Foundation (grant number 155/18), and the Binational Science Foundation (grant number 2016376).

AI declaration: While preparing this work, the authors used ChatGPT to improve the readability

and language of the work. After using this tool, we reviewed and edited the content as needed and took full responsibility for the paper's content.

Appendix A: Relation between eGR and iGR:

Given the time-lapse trajectories of cell size (or equivalently, the mass), $V(t)$, we define the instantaneous growth (iGR) rate as

$$\alpha(t) = \frac{1}{V}\frac{dV}{dt}, \tag{A1}$$

which is the relative rate of change of cell size.

On the other hand, we observe that cell size fits an exponential growth pattern across the continuous growth between successive divisions. One may define the approximately constant exponential growth rate over each cell cycle, the effective growth rate (eGR), by fitting. In this approximation, the best-fit rate over the cycle is also equal to the average of $\alpha(t)$

$$\lambda = \frac{1}{T}\ln\left(\frac{V_d}{V_b}\right), \tag{A2}$$

where T indicates the duration of the cell cycle, V_d is the cell size at the time of division and V_b is cell size at birth. The noise in eGR is variability in λ_n across different cell cycles n. We quantify this noise by the coefficient of variation (CV), which is the ratio of standard deviation and mean calculated across cycles.

By comparing Eqs. (A1) and (A2), it is easy to see

$$\lambda = \frac{1}{T}\int_0^T \alpha(t)dt = \langle\alpha\rangle_t, \tag{A3}$$

implying eGR is the temporal mean of the iGR over the duration T of the cell cycle. Despite fluctuations and deviations from a perfect exponential over the cycle, our empirical observations on *E. coli* substantiate this simple math, revealing a robust correlation between eGR and the time-averaged iGR, as depicted in Fig.2b (insert). Additionally, their distribution patterns' alignment is illustrated in Fig. 2b.

Appendix B: Fixed point analysis of metabolic network Eq. 5

The dynamic equations for the concentrations of species in the network are given as follows

$$\dot{Y}_{aa} = k_1 Y_e - (k_2 + k_3)\, Y_{aa} Y_r - \alpha(\mathbf{Y}) Y_{aa} \tag{B1a}$$

$$\dot{Y}_e = k_2 Y_{aa} Y_r - \alpha(\mathbf{Y}) Y_e, \tag{B1b}$$

$$\dot{Y}_r = k_3 Y_{aa} Y_r - \alpha(\mathbf{Y}) Y_r, \tag{B1c}$$

with fixed point found by setting $\dot{Y}_i = 0$ as follows

$$\overline{Y_{aa}} = \frac{\overline{\alpha}}{k_3}, \tag{B2}$$

$$\overline{Y_r} = \frac{\overline{\alpha}^2}{k_1 k_2 - (k_2 + k_3)\overline{\alpha}}, \tag{B3}$$

$$\overline{Y_e} = \overline{Y_r}\frac{k_2}{k_3}. \tag{B4}$$

The explicit expression for iGR at the fixed point will be a function of concentrations at this point

$$\overline{\alpha} = k_1 \rho_{aa} \overline{Y_e} + (k_2 \rho_e + k_3 \rho_r - (k_2 + k_3)\rho_{aa})\overline{Y}_{aa}\overline{Y_r}. \tag{B5}$$

Eqs. (B2-B5) can be combined to obtain the iGR of a cell at the fixed point as a function of model parameters,

$$\overline{\alpha} = \frac{-(k_2 k_3 + k_3^2 + k_1 k_2 \rho_{aa}) + \sqrt{(k_2 k_3 + k_3^2 + k_1 k_2 \rho_{aa})^2 + 4 k_1 k_2 k_3 (k_2 \rho_e + k_3 \rho_r - (k_2 + k_3)\rho_{aa})}}{2(k_2 \rho_e + k_3 \rho_r - (k_2 + k_3)\rho_{aa})}. \tag{B6}$$

The numerator of this expression will be negative when $(k_2 \rho_e + k_3 \rho_r - (k_2 + k_3)\rho_{aa}) < 0$, which in turn makes the denominator also negative. As a result $\overline{\alpha}$ will be positive for all positive rate parameters, showing explicitly that the attractor is of an exponentially growing nature. In the special case of $\rho_{aa} = \rho_e = \rho_r$, i.e., if we assume the equal contribution from each species to the cell size, then the steady-state iGR will be expressed in a simpler mathematical form as follows

$$\overline{\alpha} = \frac{k_1 k_2 k_3}{k_1 k_2 + k_3(k_2 + k_3)}. \tag{B7}$$

Our next step is to analyze the linear stability of fixed point $\{\overline{Y}_{aa}, \overline{Y}_e, \overline{Y}_r\}$ in the concentration space. This stability is determined by the eigenvalues of the Jacobian matrix evaluated at the fixed point as follows

$$J = \begin{pmatrix} \frac{\partial f}{\partial Y_{aa}} & \frac{\partial f}{\partial Y_e} & \frac{\partial f}{\partial Y_r} \\ \frac{\partial g}{\partial Y_{aa}} & \frac{\partial g}{\partial Y_e} & \frac{\partial g}{\partial Y_r} \\ \frac{\partial h}{\partial Y_{aa}} & \frac{\partial h}{\partial Y_e} & \frac{\partial h}{\partial Y_r} \end{pmatrix} \tag{B8}$$

where the functions f, g, h are the right hand side of Eqs. (B1) respectively. The Jacobian matrix represents the system's linear approximation near the fixed point, and its eigenvalues give information about the local dynamics. If the eigenvalues are real negative then the fixed point is stable, i.e., following perturbations the trajectories will relax back to it. The magnitude of these real parts gives a measure of how quickly this relaxation occurs, where larger magnitudes mean faster relaxation. One can obtain an exact mathematical form of the eigenvalues $\{\mathcal{E}_1, \mathcal{E}_2, \mathcal{E}_3\}$ for

this reaction network as follows

$$\mathcal{E}_1 = -\overline{\alpha}, \tag{B9}$$

$$\mathcal{E}_2 = -\overline{\alpha}, \tag{B10}$$

$$\mathcal{E}_3 = -\left(\frac{(\overline{\alpha}^2\rho_{aa} - 2\overline{\alpha}k_3)\left[\rho_{aa}(k_2+k_3) - (k_2\rho_e + k_3\rho_r)\right] + k_3^2(k_3+k_2)}{k_3(k_2\rho_e + k_3\rho_r)}\right), \tag{B11}$$

where $\overline{\alpha}$ is given in Eq. (B6). In the special case of $\rho_{aa} = \rho_e = \rho_r$, i.e., if we assume the equal contribution from each species to the cell size, then the third eigenvalue $\mathcal{E}_3 = -k_3$, which is real negative. The eigenvalues $\{\mathcal{E}_1, \mathcal{E}_2, \mathcal{E}_3\}$ are real negative, signifying the fixed point is stable. The absolute values of two of these eigenvalues are increasing functions of the steady-state growth rate $\overline{\alpha}$, indicating that cells with a faster growth rate will converge to the fixed point faster.

Appendix C: Flow map in $\alpha - \dot{\alpha}$ plane for different experimental conditions

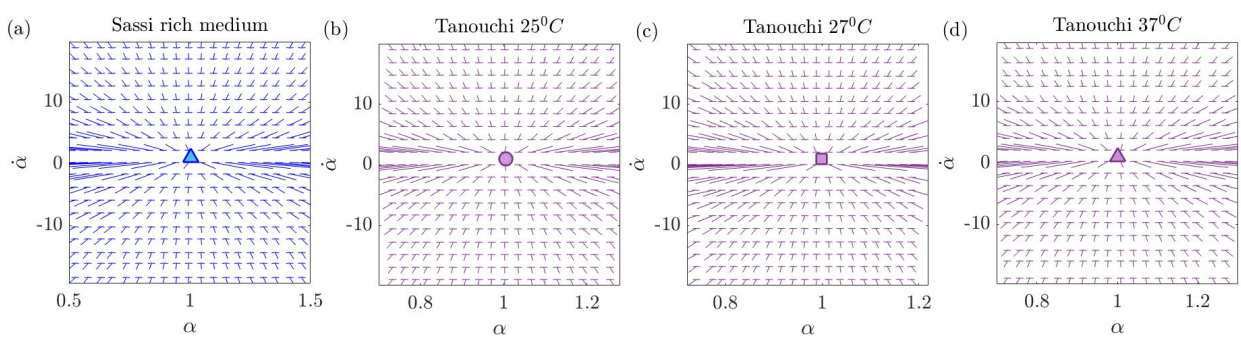

FIG. S1. **Experimental data exhibit stable node attractor dynamics in $\alpha - \dot{\alpha}$ plane.** Experimental data on *E. coli* growing in **(a)** nurient rich medium (9) and **(b-d)** different temperature (12): A flow map is estimated in the 2D phase space $\alpha - \dot{\alpha}$. Arrows indicate the flow direction. The markers are the stable node attractors on this projection of the dynamics. A flow map in the iGR phase space, generated by discretizing α and $\dot{\alpha}$ into 20 bins. Arrows, originating from bin averages of α and $\dot{\alpha}$, indicate changes between consecutive bins. Each vector is normalized to clearly and uniformly represent the directional field in the $\alpha - \dot{\alpha}$ phase plane, without scaling distortion. Experimental details are provided in Table II.

Appendix D: Protein copy number threshold

Instead of cell size threshold, we will consider a certain protein number as a threshold quantity for the same growth model as discussed in the main text Eq. (5). We denote this protein as a "threshold protein". A cell will divide when the number of "threshold protein" Z reaches a stochastic threshold value. The dynamics of Z is

$$\dot{Z} = k_Z \frac{X_{aa} X_r}{V}, \tag{D1}$$

which has a negligible effect on the dynamics of other components (25). The schematic of this

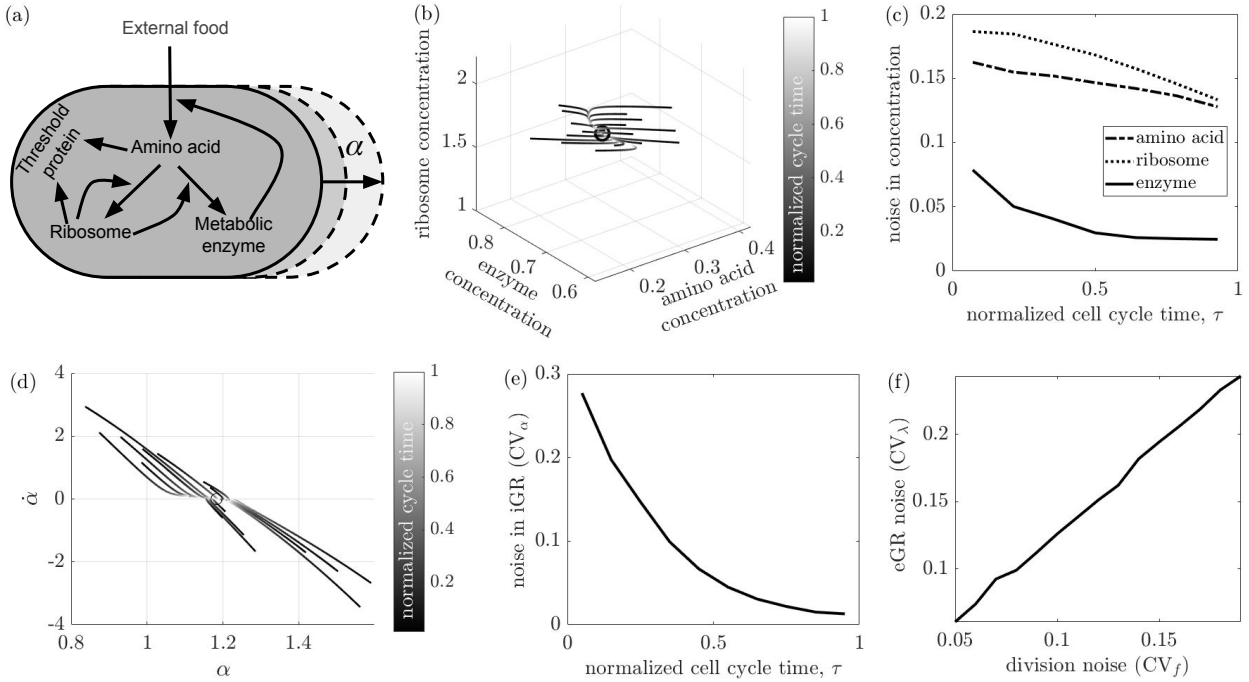

FIG. S2. **Protein number threshold provides similar results as cell size threshold. (a)** Schematic of nonlinear reactions within a cell that grows with rate α. The threshold is on the copy number of the "Threshold protein" synthesized from the amino acids in reactions catalyzed by ribosomes. **(b)** Cell trajectories in the concentration phase space of three species and **(d)** $\alpha - \dot{\alpha}$ plane with division noise of $\mathrm{CV}_f = 0.15$ while the threshold noise is fixed at 0.15. These trajectories are color-coded by normalized cell cycle time from 0 (black, cycle start) to 1 (white, cycle end). Noise in **(c)** concentrations of three species and **(e)** iGR decreases over the cell cycle. **(f)** The noise in eGR increases with division noise.

model is presented in Fig. S2 (a). The threshold value is considered stochastic in our analysis that follows a Gaussian distribution with a finite mean and variance. The noise in the threshold is described by the CV of that Gaussian distribution. The simulated results from this threshold model are presented in Fig. S2. Like the cell size threshold in the main text here also a dynamic attractor exists showing a stable fixed point in the phase space of concentrations (Fig. S2b) and iGR (Fig. S2d). Due to the underlying dynamic attractor the noise in both concentration and iGR decrease over the cell cycle as presented respectively in Figs. S2 (c) and (e). However, noise from the uneven division kicks the system out of the stable fixed point inducing noise in the growth rate, which increases with the division noise (Fig. S2 f).

Appendix E: Hinshelwood Cycle Model

We consider another growth model, where the production of each species X_i is catalyzed by its predecessor X_{i-1} at rate $k_i X_{i-1}$, known as deterministic Hinshelwood cycle (DHC). The Stochastic

Hinshelwood Cycle (SHC) extends the DHC by assuming exponentially distributed waiting times for each reaction (21, 29). If we consider three species then the number of dynamics of each species

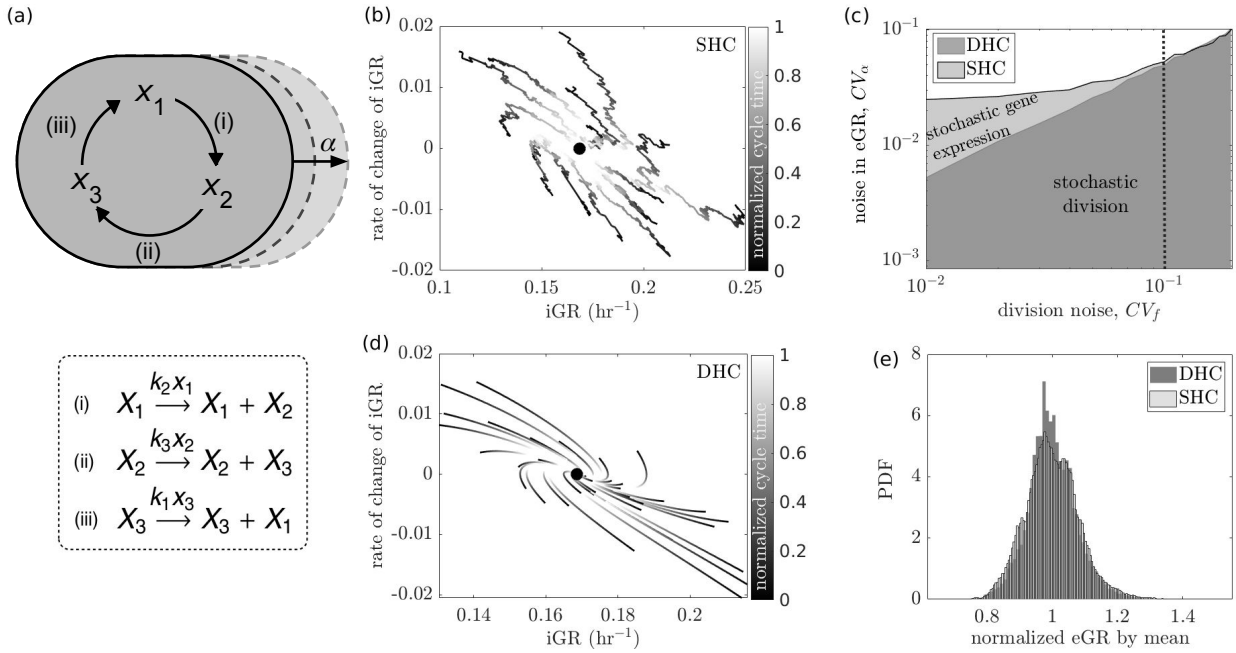

FIG. S3. **Negligible impact of stochastic gene expression noise on growth rate fluctuations.** **(a)** Illustrates the Deterministic Hinshelwood Cycle (DHC) within a growing cell at rate α, showcasing an example with three chemical species. Production of each species X_i is catalyzed by its predecessor X_{i-1} at rate $k_i X_{i-1}$, with the reactions detailed in the inset. The Stochastic Hinshelwood Cycle (SHC) extends the DHC by assuming exponentially distributed waiting times for each reaction as previously studied (21, 29). Gillespie simulation is used (35) on Eq. (E1) for SHC model. Division events are modeled as cell size threshold-crossing processes with division noise CV_f. Time-lapse simulations of the iGR and its rate of change over a cell cycle under division noise of magnitude 0.15 are shown for **(b)** SHC and **(d)** DHC. Trajectories in these simulations are color-coded based on normalized cell cycle time, transitioning from black at the cycle's commencement to white at its conclusion. Notably, all trajectories converge to a fixed point (black circle) by the end of the cycle, indicative of the cell's behavior as a dynamical attractor in both SHC and DHC models. **(c)** Demonstrates that the CV, calculated as the ratio of standard deviation to mean of the effective growth rate (eGR) for both DHC and SHC, is identical and increases with division noise. This finding suggests that intrinsic noise in the SHC model does not significantly alter eGR fluctuations, even in the presence of division noise. **(e)** Displays PDFs of eGR for both DHC and SHC at the division noise level of 0.15 (indicated by the black dotted line in plot **c**). The PDFs from both models are remarkably similar, further supporting the negligible effect of intrinsic noise on eGR variability. Parameter values: $k_1 = 0.1$, $k_2 = 0.15$, $k_3 = 0.32$, $\rho_1 = 0.05$, $\rho_2 = 1.6$, $\rho_3 = 0.5$.

and cell volume will be

$$\dot{X_1} = k_1 X_3, \tag{E1}$$

$$\dot{X_2} = k_2 X_1, \tag{E2}$$

$$\dot{X_3} = k_3 X_2, \tag{E3}$$

$$V(t) = \rho_1 X_1 + \rho_2 X_2 + \rho_3 X_3. \tag{E4}$$

This model schematic is depicted in Fig. S3(a). For these models, we also consider division as a threshold-crossing model, i.e., a cell will divide when $V(t) \geq V_c$. Our simulation of both DHC and SHC models also showcases the dynamic attractor picture as plotted in Fig. S3(b) and (d).

Appendix F: Experimental details of filamenting cells

Measurements of filamentous growth of cells were carried out using the *E. coli* K-12 derivative MG1655. Cells were transfected with two plasmids, pZA3R-mcherry - expressing a red fluorescent protein under the control of the λ-phage Pr promoter, and pRJ2001-GFP-Fis - expressing the DNA-binding protein Fis fused with GFP under the control of the lac promoter. The former plasmid was used to enable better imaging of the cell, and the latter was added to ensure that DNA was replicated during the filamentation of cells. Bacterial cultures were initiated from frozen stock and grown overnight in LB medium at 32^0C. The following day, the cultures were diluted in the same medium and regrown until reaching an Optical Density (OD) $\sim$0.1. They were then concentrated to an OD of 0.3 in fresh LB medium and loaded into the microfluidic device, the mother machine. Trapped cells were allowed to grow in the channels for 24 hours while supplied with LB medium flowing through the device at a rate of 1 ml/hr. Following the 24 hours of normal growth, the supplied medium was exchanged with LB containing 5μg/ml cephalexin, which induced the filamentation of the trapped bacteria. Images of the bacteria were acquired in DIC and fluorescence modes every 3 minutes during the entire experiment using a Hamamatsu ORCA-flash4.0 camera, mounted on a Nikon Eclipse Ti2 inverted microscope with a 100X objective. An Okolab microscope enclosure was used to maintain the temperature at 32^0C. Cell length was then extracted from the acquired images using Oufti64 and custom-made MATLAB codes.

Appendix G: Cell size noise across cycle

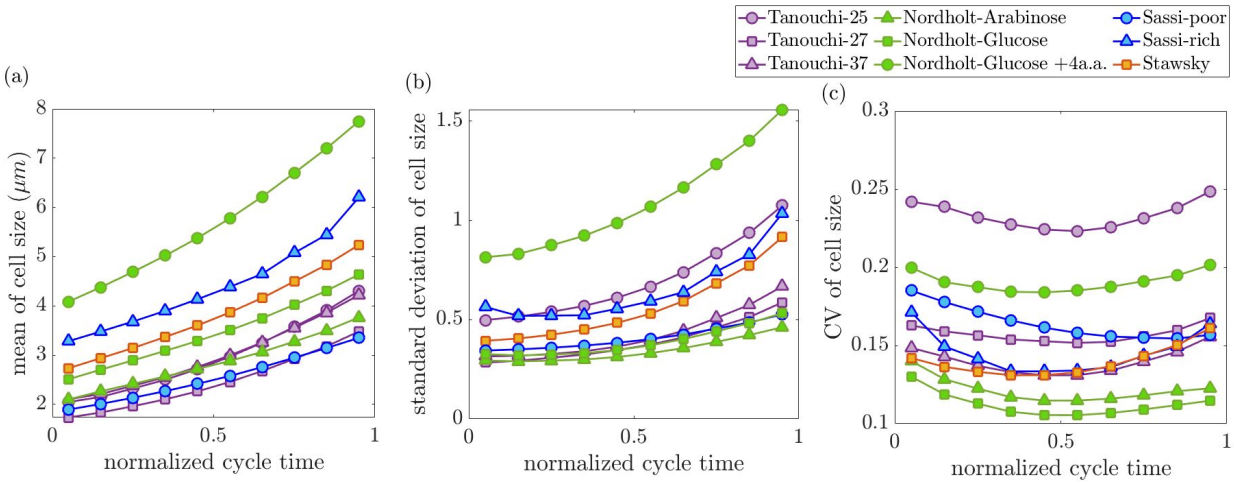

FIG. S4. **Statistical properties of cell size across cycle from *E. coli* data.** Variation of **(a)** mean, **(b)** standard deviation, and **(c)** noise (CV) of cell size across normalized cell cycle time obtained from *E. coli* (9, 12, 24) and *B. subtilis* data (18). Experimental details are provided in Table II.

Appendix H: Parameter details for figures

Parameters	Values	Parameters	Values
$\langle V_c \rangle$: Average size threshold	10 μm	CV_c: noise of size threshold	0.15
$\langle f \rangle$: Average division fraction	0.5	CV_f: noise of division fraction	0.15
k_1: Metabolic rate of amino acid production	4 hr^{-1} for others 1-8 hr^{-1} for Fig. 5(b)	k_2: Catalytic rate of enzyme production	2 hr^{-1}
k_3: Catalytic rate of ribosome production	4 hr^{-1}	ρ_{aa}: Molar vol. of amino acid	1.3
ρ_r: Molar vol. of ribosomes	0.25	ρ_e: Molar vol. of metabolic enzyme	0.65

TABLE I. Parameter values for Figs. (3), (4), and (5)

Strain	Media Name	#cell cycles	Temperature	average birth size (μm)	average growth rate (min^{-1})	References
E. coli in NCM3722 background	glycerol	1.12×10^4	37 ^0C	2.07	0.0189	(13)
	sorbitol	7439		2.26	0.0187	
	glucose	1.25×10^4		2.1	0.0270	
	glucose + 6 a.a.	1.68×10^4		2.35	0.0330	
	glucose + 12 a.a.	1.33×10^4		2.87	0.0372	
	Synthetic rich	1.09×10^4		3.33	0.0433	
	Tryptic soy broth	1.11×10^4		3.98	0.0569	
E. coli in NCM3722 background	arginine	1701	37 ^0C	1.48	0.0067	(17)
	glucose + 12 a.a.	1464		2.82	0.0234	
	glucose	1432		1.89	0.0144	
E. coli in MG1655 background	M9 acetate	1554		1.88	0.0034	
	glucose	1807		2.51	0.0131	
	glycerol + 11 a.a.	1491		2.67	0.0109	
E. coli in MC4100 background	LB minimal	4550	25 ^0C	1.96	0.0121	(12)
		3780	27 ^0C	1.64	0.0149	
		1.12×10^4	37 ^0C	1.98	0.0253	
B. subtilis	arabinose	1.58×10^4	37 ^0C	2.07	0.0062	(18)
	glucose	1.25×10^4		2.477	0.0108	
	glucose + 4 a.a.	2887		4.105	0.0133	
E. coli in MG1655 background	poor	9.56×10^4	30 ^0C	1.93	0.0086	(9)
	rich (RDM)	4.64×10^4		3.28	0.0153	
E. coli in STK13 background	alanine-TrEl	215	28 ^0C	1.75	0.0033	(19)
	glucose-Cas	409		2.01	0.0099	
	mannose	401		1.5	0.0035	
	glucose	344		1.8	0.0061	
	glycerol-Cas	420		1.9	0.0074	
	glycerol-TrEl	423		1.61	0.0046	
	glycerol	302		1.7	0.0042	
E. coli in JM85 background	glucose-Cas	406		2.1	0.0092	
	glycerol	388		2.01	0.0044	
Wild type MG1655 *E. coli* under the control of *lac* promoter	M9 minimal	381	30 ^0C	2.31	0.0229	(8)
Wild type MG1655 *E. coli*	LB minimal	4096	30 ^0C	2.65	0.0357	(16)
Wild type MG1655 *E. coli* under the control of λ promoter	M9 minimal	1794		1.35	0.0509	
	LB minimal	3551		2.78	0.0252	
Wild type MG1655 *E. coli* under the control of *lac* promoter	M9 minimal	562		2.43	0.0233	
Wild type MG1655 *E. coli* under the control of both λ & *lac* promoter	LB minimal	188		1.21	0.0257	

TABLE II. List of growth media, temperature, strains, number of total cell cycles, mean birth size and mean growth rate for several experiments used in our manuscript.

[1] O. Rahn, "A chemical explanation of the variability of the growth rate," *The Journal of general physiology*, vol. 15, no. 3, pp. 257–277, 1932.

[2] E. Powell, "An outline of the pattern of bacterial generation times," *Microbiology*, vol. 18, no. 2, pp. 382–417, 1958.

[3] N. Brenner, K. Farkash, and E. Braun, "Dynamics of protein distributions in cell populations," *Physical Biology*, vol. 3, no. 3, p. 172, 2006.

[4] D. Huh and J. Paulsson, "Non-genetic heterogeneity from stochastic partitioning at cell division," *Nature genetics*, vol. 43, no. 2, pp. 95–100, 2011.

[5] H. Salman, N. Brenner, C.-k. Tung, N. Elyahu, E. Stolovicki, L. Moore, A. Libchaber, and E. Braun, "Universal protein fluctuations in populations of microorganisms," *Physical review letters*, vol. 108, no. 23, p. 238105, 2012.

[6] K. Hosoda, T. Matsuura, H. Suzuki, and T. Yomo, "Origin of lognormal-like distributions with a common width in a growth and division process," *Physical Review E*, vol. 83, no. 3, p. 031118, 2011.

[7] A. Amir, "Cell size regulation in bacteria," *Physical review letters*, vol. 112, no. 20, p. 208102, 2014.

[8] N. Brenner, E. Braun, A. Yoney, L. Susman, J. Rotella, and H. Salman, "Single-cell protein dynamics reproduce universal fluctuations in cell populations," *The European Physical Journal E*, vol. 38, no. 9, pp. 1–9, 2015.

[9] A. S. Sassi, M. Garcia-Alcala, M. Aldana, and Y. Tu, "Protein Concentration Fluctuations in the High Expression Regime: Taylor's Law and Its Mechanistic Origin," *Physical review X*, vol. 12, no. 1, p. 011051, 2022.

[10] K. Biswas and N. Brenner, "Universality of phenotypic distributions in bacteria," *Physical Review Research*, vol. 6, no. 2, p. L022043, 2024.

[11] P. Wang, L. Robert, J. Pelletier, W. L. Dang, F. Taddei, A. Wright, and S. Jun, "Robust growth of Escherichia coli," *Current biology*, vol. 20, no. 12, pp. 1099–1103, 2010.

[12] Y. Tanouchi, A. Pai, H. Park, S. Huang, R. Stamatov, N. E. Buchler, and L. You, "A noisy linear map underlies oscillations in cell size and gene expression in bacteria," *Nature*, vol. 523, no. 7560, pp. 357–360, 2015.

[13] S. Taheri-Araghi, S. Bradde, J. T. Sauls, N. S. Hill, P. A. Levin, J. Paulsson, M. Vergassola, and S. Jun, "Cell-size control and homeostasis in bacteria," *Current biology*, vol. 25, no. 3, pp. 385–391, 2015.

[14] M. Wallden, D. Fange, E. G. Lundius, Ö. Baltekin, and J. Elf, "The synchronization of replication and division cycles in individual E. coli cells," *Cell*, vol. 166, no. 3, pp. 729–739, 2016.

[15] D. Yang, A. D. Jennings, E. Borrego, S. T. Retterer, and J. Männik, "Analysis of factors limiting bacterial growth in PDMS mother machine devices," *Frontiers in microbiology*, vol. 9, p. 871, 2018.

[16] L. Susman, M. Kohram, H. Vashistha, J. T. Nechleba, H. Salman, and N. Brenner, "Individuality and slow dynamics in bacterial growth homeostasis," *Proceedings of the National Academy of Sciences*, vol. 115, no. 25, pp. E5679–E5687, 2018.

[17] F. Si, G. Le Treut, J. T. Sauls, S. Vadia, P. A. Levin, and S. Jun, "Mechanistic origin of cell-size control and homeostasis in bacteria," *Current Biology*, vol. 29, no. 11, pp. 1760–1770, 2019.

[18] N. Nordholt, J. H. van Heerden, and F. J. Bruggeman, "Biphasic cell-size and growth-rate homeostasis by single bacillus subtilis cells," *Current Biology*, vol. 30, no. 12, pp. 2238–2247, 2020.

[19] S. Tiruvadi-Krishnan, J. Männik, P. Kar, J. Lin, A. Amir, and J. Männik, "Coupling between DNA replication, segregation, and the onset of constriction in Escherichia coli," *Cell reports*, vol. 38, no. 12, p. 110539, 2022.

[20] J. Grilli, C. Cadart, G. Micali, M. Osella, and M. Cosentino Lagomarsino, "The empirical fluctuation pattern of E. coli division control," *Frontiers in microbiology*, vol. 9, p. 1541, 2018.

[21] S. Iyer-Biswas, C. S. Wright, J. T. Henry, K. Lo, S. Burov, Y. Lin, G. E. Crooks, S. Crosson, A. R. Dinner, and N. F. Scherer, "Scaling laws governing stochastic growth and division of single bacterial cells," *Proceedings of the National Academy of Sciences*, vol. 111, no. 45, pp. 15912–15917, 2014.

[22] N. Brenner, C. Newman, D. Osmanović, Y. Rabin, H. Salman, and D. Stein, "Universal protein distributions in a model of cell growth and division," *Physical Review E*, vol. 92, no. 4, p. 042713, 2015.

[23] A. Cylke and S. Banerjee, "Super-exponential growth and stochastic size dynamics in rod-like bacteria," *Biophysical Journal*, vol. 122, no. 7, pp. 1254–1267, 2023.

[24] A. Stawsky, H. Vashistha, H. Salman, and N. Brenner, "Multiple timescales in bacterial growth homeostasis," *Iscience*, vol. 25, no. 2, p. 103678, 2022.

[25] P. P. Pandey, H. Singh, and S. Jain, "Exponential trajectories, cell size fluctuations, and the adder property in bacteria follow from simple chemical dynamics and division control," *Physical Review E*, vol. 101, no. 6, p. 062406, 2020.

[26] P. Thomas, G. Terradot, V. Danos, and A. Y. Weiße, "Sources, propagation and consequences of stochasticity in cellular growth," *Nature communications*, vol. 9, no. 1, p. 4528, 2018.

[27] J. J. Tyson and O. Diekmann, "Sloppy size control of the cell division cycle," *Journal of theoretical biology*, vol. 118, no. 4, pp. 405–426, 1986.

[28] C. N. Hinshelwood, "136. on the chemical kinetics of autosynthetic systems," *Journal of the Chemical Society (Resumed)*, pp. 745–755, 1952.

[29] S. Iyer-Biswas, G. E. Crooks, N. F. Scherer, and A. R. Dinner, "Universality in stochastic exponential growth," *Physical review letters*, vol. 113, no. 2, p. 028101, 2014.

[30] W.-H. Lin, E. Kussell, L.-S. Young, and C. Jacobs-Wagner, "Origin of exponential growth in nonlinear reaction networks," *Proceedings of the National Academy of Sciences*, vol. 117, no. 45, pp. 27795–27804, 2020.

[31] P. P. Pandey and S. Jain, "Analytic derivation of bacterial growth laws from a simple model of intracellular chemical dynamics," *Theory in Biosciences*, vol. 135, pp. 121–130, 2016.

[32] J. Lin and A. Amir, "Homeostasis of protein and mRNA concentrations in growing cells," *Nature communications*, vol. 9, no. 1, p. 4496, 2018.

[33] D. H. de Groot, J. Hulshof, B. Teusink, F. J. Bruggeman, and R. Planqué, "Elementary growth modes provide a molecular description of cellular self-fabrication," *PLoS computational biology*, vol. 16, no. 1, p. e1007559, 2020.

[34] I. Gelber, A. Aranovich, M. Feingold, and I. Fishov, "Stochastic nucleoid segregation dynamics as a source of the phenotypic variability in E. coli," *Biophysical Journal*, vol. 120, no. 22, pp. 5107–5123, 2021.

[35] D. T. Gillespie, "Exact stochastic simulation of coupled chemical reactions," *The journal of physical chemistry*, vol. 81, no. 25, pp. 2340–2361, 1977.

[36] H. Vashistha, M. Kohram, and H. Salman, "Non-genetic inheritance restraint of cell-to-cell variation," *Elife*, vol. 10, p. e64779, 2021.

[37] X. Liu, J. Yan, and M. W. Kirschner, "Cell size homeostasis is tightly controlled throughout the cell cycle," *PLoS Biology*, vol. 22, no. 1, p. e3002453, 2024.